2008

Effect of Nb and Mo Additions on the Microstructure and Mechanical Properties of Thermomechanically Processed and Bake Hardened CMnSi Trip Steel

E V. Pereloma
University of Wollongong, elenap@uow.edu.au

I. B. Timokhina
Monash University

M. K. Miller
Oak Ridge National Laboratory, US

EFFECT OF Nb AND Mo ADDITIONS ON THE MICROSTRUCTURE AND MECHANICAL PROPERTIES OF THERMOMECHANICALLY PROCESSED AND BAKE HARDENED CMnSi TRIP STEEL

E.V. Pereloma[1], I.B. Timokhina[2] and M.K. Miller[3]

[1]School of Mechanical, Materials and Mechatronics Engineering, University of Wollongong, NSW 2522, Australia
[2]Department of Materials Engineering, Monash University, VIC 3800, Australia
[3]Materials Science and Technology Division, Oak Ridge National Laboratory, TN 37831-6136, USA

Keywords
Transformation-induced plasticity steels, bake hardening, three-dimensional atom probe, clustering, Cottrell atmospheres, precipitation

Abstract
Bake hardening of steels during paint baking of an automotive body could result in an increase of their strength. In this work, the effect of pre-straining and bake-hardening on the microstructure and mechanical properties has been investigated in thermomechanically processed CMnSi Transformation-Induced Plasticity (TRIP) steels with and without additions of Nb and Mo. The steels were characterised before and after bake hardening at 180^{o}C for 30 min. by transmission electron microscopy (TEM), X-ray diffraction (XRD), atom probe tomography (APT), and tensile tests.

The microstructure of the thermomechanically processed (TMP) TRIP steels consisted of polygonal ferrite, bainite, retained austenite and martensite. Fine Nb and Mo carbides were detected by TEM in the microstructure of the alloyed steel. In addition, APT revealed the presence of Nb-, Mo-, Fe-, C-containing clusters. Cottrell atmospheres were also detected in the ferrite phase of the CMnSi steel. After pre-straining and bake hardening (PS/BH) both steels exhibit continuous yielding behaviour. The observed higher yield and tensile strengths of the PS/BH samples in comparison with the TMP samples were due to an increase in the number density of dislocations and their interaction with iron carbides formed in bainite and martensite. In addition, the number density of fine Nb and Mo carbides was significantly increased in the alloyed TRIP steel after PS/BH, which also contributed to significant precipitation strengthening in the NbMo steel.

Introduction
Thermomechanically processed C-Mn-Si Transformation-Induced Plasticity (TRIP) steels exhibit an excellent combination of strength (700-1000 MPa) and ductility (30-40% total elongation) [1]. The interaction of all phases present in the microstructure (polygonal ferrite, carbide-free bainite, retained austenite and martensite) during deformation and the deformation-induced transformation of the metastable retained austenite to martensite at room temperature [2-4] are thought to be responsible for these mechanical properties. These TRIP steels could be possible candidates for automotive applications. Additional alloying with Nb and/or Mo provides the further strength increase through an increase in hardenability, microstructure refinement and precipitation strengthening [5,6]. During paint baking of an automotive body, the steels are strain aged, which results in a further increase in yield strength of ~100-200 MPa and improved dent and crash resistance [7]. Recently, research on bake hardening of intercritically annealed CMnSi TRIP steels has shown an increase in yield strength and the appearance of yield point after 2-10% pre-straining and baking at 170-180 ^{o}C for 20-30 min. [5, 8-11]. The discontinuous yielding behaviour is undesirable in auto body applications. Limited work on

bake hardening of thermomechanically processed TRIP steels also has shown an increase in the yield and tensile strengths, but it is accompanied by continuous yielding behaviour [11,12], which indicates a difference in the bake hardening mechanisms operating in these steels.

This paper addresses the effect of post-processing on the microstructure and mechanical properties of thermomechanically processed CMnSi TRIP steels with and without Nb and Mo additions. In particular, attention is given to the characterisation of solute segregation and nanosize particles by atom probe tomography.

Experimental

Two steels with compositions given in Table 1 were subjected to thermomechanical processing simulations using a laboratory rolling mill at Deakin University. The details of the processing schedule are described elsewhere [3,12]. The selected parameters are given in Table 1. After the simulation of coiling in a fluidized bed furnace, the samples were quenched to room temperature. Tensile specimens were machined from the strip and subjected to 4% pre-straining (PS) before bake hardening (BH) at 180 ^{o}C for 30 min. Room temperature mechanical properties of the samples after TMP and TMP/BH/PS were determined with an Instron 4500 servohydraulic tensile testing machine with a 100 kN load cell. The resultant microstructures were characterised with a Philips CM20 transmission electron microscope operated at 200kV and an Imago Scientific Instruments local electrode atom probe (LEAP®). The samples for both studies were cut perpendicular to the deformation (rolling) direction. TEM thin foils were prepared by twin jet electropolishing using a solution of 5% perchloric acid in methanol at –20 °C with an operating voltage of 30 V. In addition, the carbon extraction replica technique was used to study precipitates in the NbMo steel. The dislocation density was calculated by counting the number of dislocation intersections (N) with random lines of length L [10]. A test line on the foil corresponds to a test area of L x t going down into the foil (where t is the foil thickness). So, the dislocation density (Λ), is given by [14]:

$$\Lambda = 2N/Lt.$$

Table1 Steel compositions and thermomechanical processing parameters

Steel		Element								Parameters		
		C	Si	Mn	Mo	Al	Cu	Nb	P	T_{AC}.^{o}C	T_{IH}, ^{o}C	t_{IH}, s
Nb Mo	wt %	0.21	1.48	1.5	0.2	0.01	0.02	0.036	0.025	735	450	1200
	at %	0.96	2.88	1.49	**0.11**	0.02	0.017	**0.021**	0.044			
non-Nb	wt %	0.21	1.55	1.55	-	0.01	0.003	0.005	-	670	450	600
	at %	0.95	3.01	1.54	-	0.02	0.003	0.003	-			

T_{AC}- accelerated cooling start temperature; T_{IH}-isothermal hold temperature, t_{IH}-holding time

The standard two-stage electropolishing procedure was used to prepare the needle-shaped atom probe specimens [13]. Atom probe analyses were performed with a sample temperature of 60 K, a pulse repetition rate of 200 kHz, and a pulse fraction of 0.2. The maximum separation envelope method with a grid spacing of 0.1 nm [13] was used to estimate the extent of the solute enriched regions (i.e., the radius of gyration, l_g) and the local compositions of these regions. Maximum separation distances, d_{max}, between the atoms of interest of 1, 0.5 and 1.5 nm were used to identify

the clusters/fine precipitates in the bainite/ferrite matrix, in the martensite/retained austenite and the solute in the atmospheres at dislocations, respectively. In order to minimize random solute fluctuations in the matrix, a minimum of 20 atoms was used to define the clusters. The Guinier radius, r_G, was calculated from $r_G = \sqrt{(5/3)}\, I_g$. It should be noted that the maximum separation method aggressively removes the solvent atoms from particles and clusters. Using the data from the maximum separation method, the observed clusters and fine carbides were grouped together based on the selection of non-overlapping ranges for their carbon content. Isoconcentration surfaces were also used to visualize the microstructural features. The amount of retained austenite in the microstructure was determined from X-ray diffraction data using a direct comparison method [15].

Results

Mechanical Properties

Both steels exhibit a good combination of strength and ductility in the thermomechanically processed state (Table 2, Fig. 1). Both steels have shown continuous yielding behaviour in all conditions (Fig. 1). Due to addition of Nb and Mo, the NbMo steel has both a higher yield strength (YS) and an ultimate tensile strength (UTS), than the non-Nb steel. However, the ductility was significantly lower than in the non-Nb steel. Post-processing led to a significant strength increase in the non-Nb steel (YS by ~280 MPa and UTS by ~90 MPa), while the total elongation decreased from ~40% to ~24%. Both YS and UTS also increased in the NbMo steel with the YS increase (~390 MPa) being significantly higher than the UTS increase (~100 MPa). At the same time, the ductility decreased from ~30 to 26% of total elongation.

Table 2 Mechanical properties of the steels.

Steel	After TMP			After post-processing		
	UTS, MPa	YS, MPa	Total El	UTS, MPa	YS, MPa	Total El
Non-Nb	910±30	520±35	0.40±0.03	1000±20	800±20	0.24±0.034
Nb-Mo	1000±20	560±20	0.3±0.02	1100±30	950±20	0.26±0.03

UTS ultimate tensile strength, YS - yield strength, El - elongation

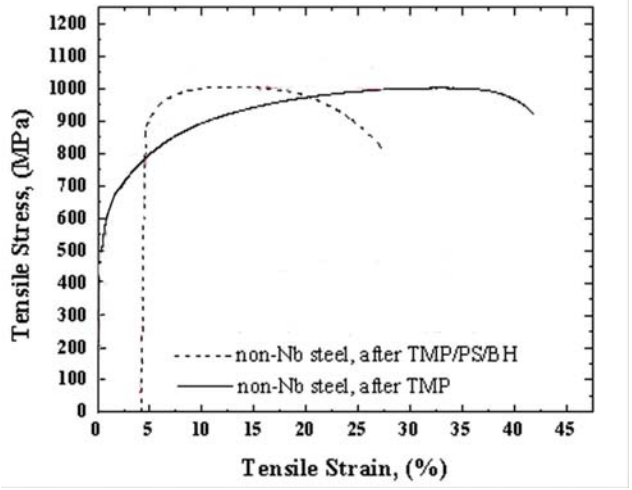

a

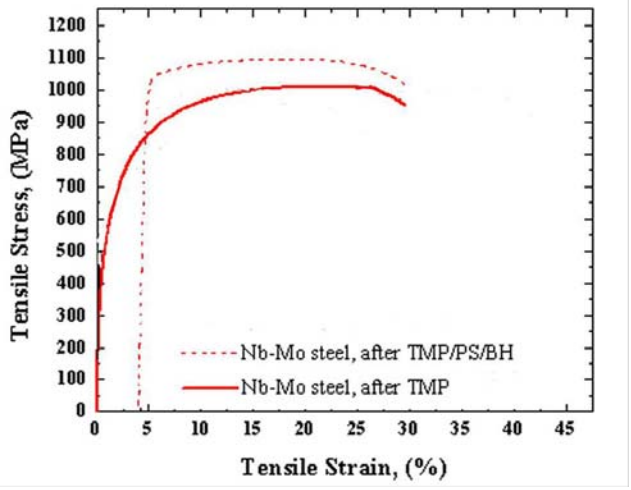

b

Fig. 1 Stress-strain curves of non-Nb steel (a) and NbMo steel (b) after various processing.

Microstructural characterisation of the non-Nb steel

In the TMP condition, the microstructure of the non-Nb steel consists of ~50±5% polygonal ferrite (PF), 14±2% retained austenite (RA) and 6±2% martensite and the remainder carbide-free bainite (Fig. 2a). The latter is predominantly granular bainite (GB), which consists of equiaxed bainitic ferrite (BF) grains with a higher dislocation density than in the PF and islands of martensite/retained austenite. The detailed microstructural characterisation is given elsewhere [3]. After PS/BH, an increase in dislocation density from (1.6 ±0.1)x$10^{14}m^{-2}$ in PF to (5.1±0.2)x$10^{14}m^{-2}$ was observed. Some of the PF grains exhibited formation of microbands (Fig. 2b), whereas twinning was detected in many martensite crystals (Fig. 2c). The PF displayed a localised work hardening behaviour in the regions adjacent to hard crystals of martensite or RA (Fig. 2d). The amount of RA was reduced to 12±0.5% after PS/BH. The presence of fine Fe_3C particles was detected in the martensite and BF matrix (Fig. 2d).

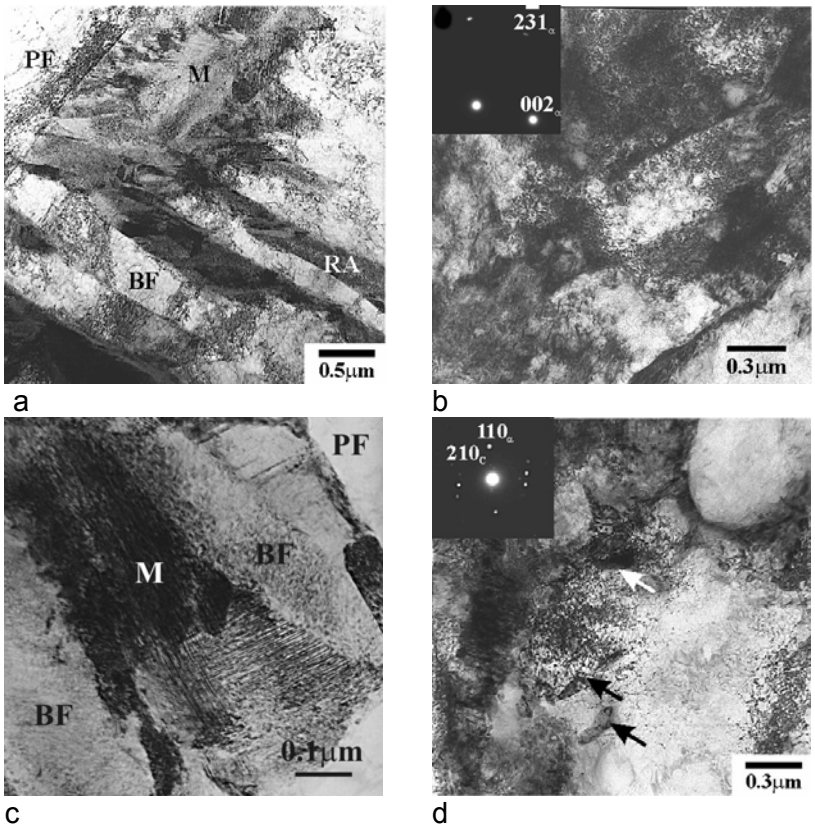

Fig. 2 Representative micrographs of the non-Nb steel after TMP (a) and after PS/BH (b-d). Zone axis is $[320]_\alpha$ in b and $[\bar{1}10]_\alpha // [\bar{1}00]_C$ in d, where α denotes bcc matrix and c denotes Fe_3C. M-martensite, BF-bainitic ferrite, PF- polygonal ferrite and RA is retained austenite. Arrows in (d) indicate iron carbides in baintic ferrite.

The formation of C atmospheres at dislocations was observed in the PF after TMP. In this study, the phases are distinguished based on their carbon content, i.e., <0.07 at % is PF, 0.1-0.3 at. %- bainite and >2 at. % martensite or RA. At the temperature of atom probe analysis, all the RA is deemed to have transformed to martensite. An example of a Cottrell atmosphere is shown in Fig. 3. A concentration profile across the atmosphere indicates that the C content at its centre is ~6 at. %. The formation of fine C clusters was observed in the martensite (Table 3, Fig. 4a).

It appears that the PS/BH treatment led to the non-uniform C segregation at dislocations (Fig. 3d, Table 3). Further decomposition of martensite with formation of Fe carbides took place during bake hardening (Figs. 4b and 4c, Table 3). Concentration profiles have indicated that the relatively coarse carbides contained up to 18-22 at. % C (Fig. 4c). The summary of effect of iron carbide size on composition is given in Fig. 4d.

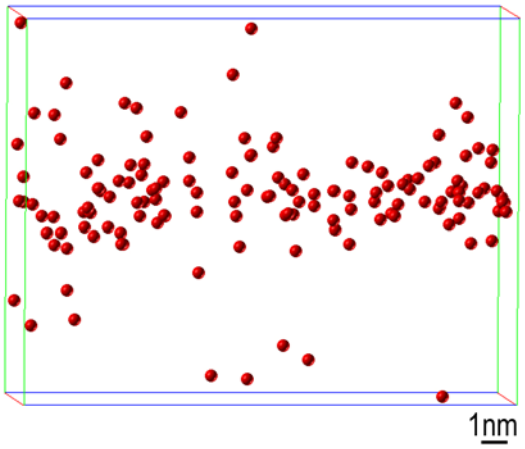

a

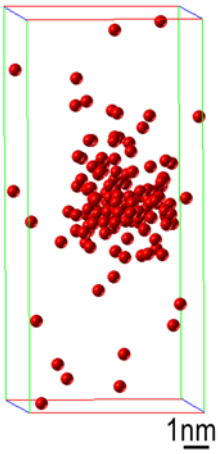

b

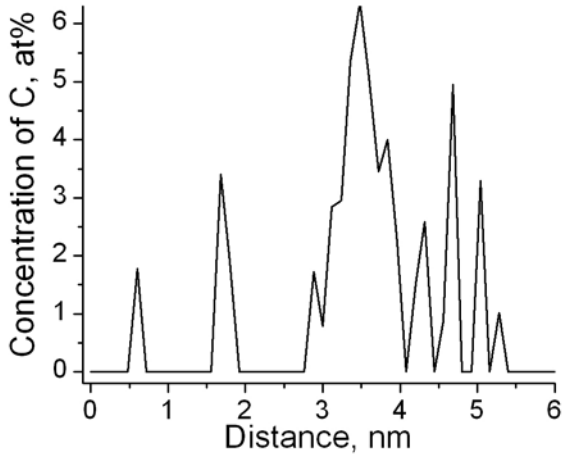

c

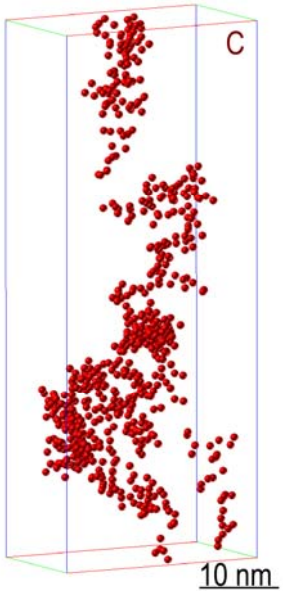

d

Fig. 3 Selected C atom maps showing the rod-like shape of a Cottrell atmosphere from two perpendicular directions (a and b) and corresponding C concentration profile taken across an atmosphere (c) in ferrite of non-Nb steel after TMP. Cottrell atmosphere after PS/BH of the non-Nb steel (d).

Table 3 Average composition, Guinier radius and number densities of the clusters and precipitates in the non-Nb steel as estimated using the maximum separation method from atom probe data.

Condition	Composition, at%			
	C	Fe	r_G, nm	N_v, m^{-3}
TMP (martensite)	100	-	0.7±0.2	1.8×10^{23}
	93.9±4.4	5.3±4.3	0.8±0.4	
	83.3±7.6	16.6±7.6	0.75	
PS/BH (PF/BF)	95.9±2.8	4.5±2.7	4.1±1.1	9.9×10^{22}
	89.3±5.9	8.9±5.3	3.9±0.3	
	79.9±1.5	18.6±1.5	10.5	
PS/BH (martensite)	100	-	0.9±0.2	2.1×10^{24}
	93.5±4.1	6.0±3.8	1.1±0.3	
	83.9±5.4	14.7±5.2	1.2±0.5	
	64.2±2.2	34±2	2.9±0.9	
	40.3±1.0	56±1*	4.3±0.9	
	24.6±0.4	70.8±0.4*	4.7±0.9	

* traces of Mn

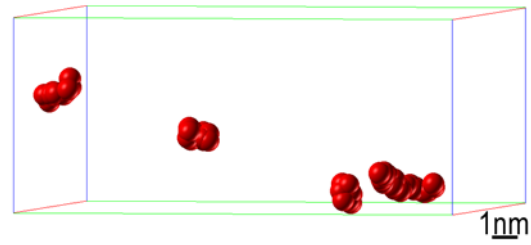

a

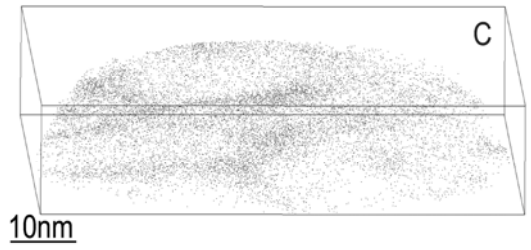

b

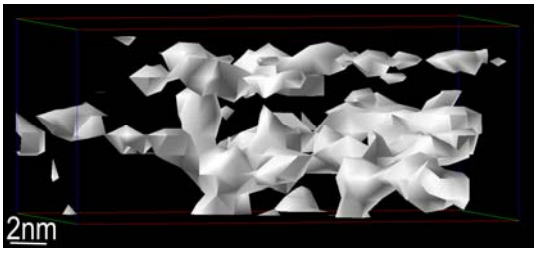

c

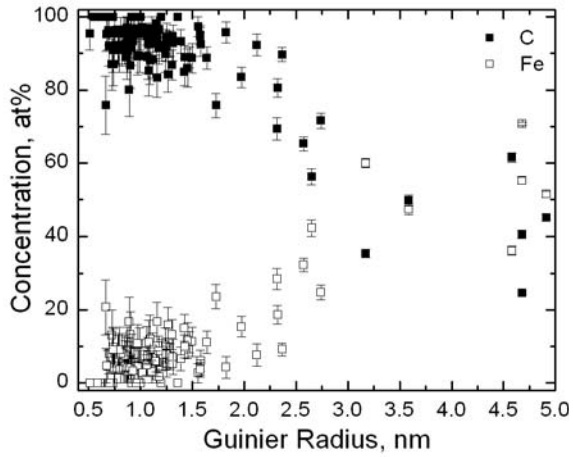

d

Fig. 4 Decomposition of martensite of the non-Nb steel after TMP (a) and after PS/BH (b-d). C atom map (b), selected 6 at. % isoconcentration surfaces (c) and summary of variation of carbide composition with size (d).

Microstructural characterisation of the NbMo steel

The microstructure of the TMP condition has been described in detail previously [16,17]. It consists of ~50% of PF, ~25% carbide-free bainitic ferrite, 12%RA and the remainder martensite (Fig. 5a). The presence of coarse (Ti,Nb)C, fine Nb-rich (Nb,Ti)C and MoC particles was detected in the steel microstructure (Figs. 5b and 5c). The PS/BH treatment resulted in an increase of dislocation density and the formation of cell structure in PF, as well as appearance of twinned martensite (Figs. 6a and 6b). Significant work hardening was detected in PF regions near hard M or RA crystals (Fig. 6a). Moreover, very fine Mo-rich and Nb-rich carbides were observed in the microstructure (Figs. 6c-e).

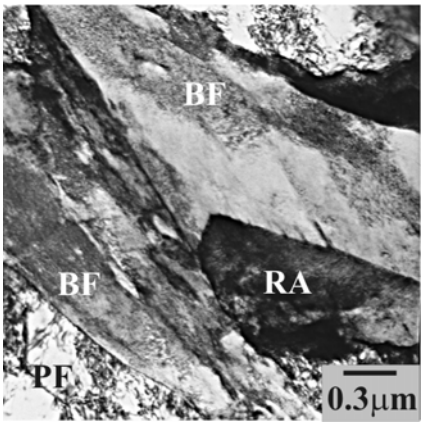

a

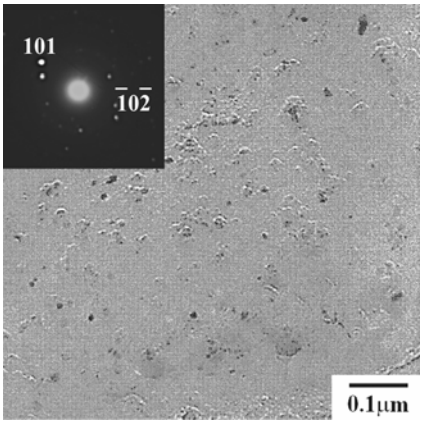

b

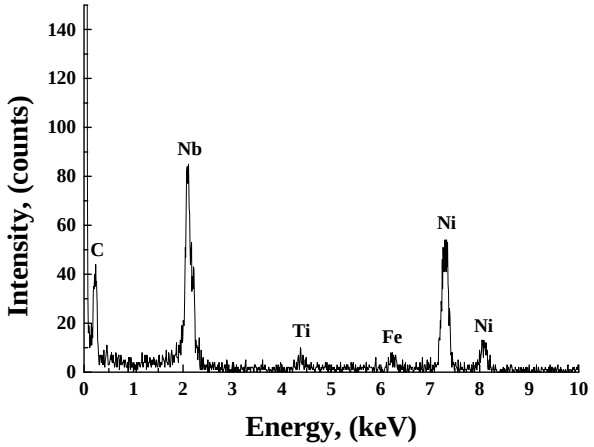

c

Fig. 5 Representative thin foil TEM (a) and carbon replica (b) showing the microstructure and precipitation in the NbMo steel after TMP, respectively. Inset in b is from a MoC particle with zone axis of [010]. Representative energy dispersive X-ray spectrometer (EDXS) spectrum from a NbC particle is shown in c. BF is bainitic ferrite, PF is polygonal ferrite and RA is retained austenite. Note: Ni peaks are from Ni grid.

APT has shown the presence of a significant number of Nb- and Mo-rich clusters in the PF and BF (Table 4, Fig. 7a) after TMP. At the same time, fine C-rich clusters were found in the martensite (Table 5). The number density of these C-rich clusters was an order of magnitude higher than the number density of the clusters in PF/BF phases. No significant effect of PS/BH treatment on clusters/fine precipitates in PF/BF phases was observed by APT. Their compositions and number density remained roughly the same (Table 4, Fig. 7b). This may be a result of the relatively limited analysed volume. The decomposition of martensite also took place in this steel with the formation of iron carbides (Fig. 8). As in the non-Nb steel, the concentration profiles across such carbides have shown a maximum concentration of 18-20 at. % C (Fig. 8c). Effect of iron carbide size on their composition is summarised in Fig. 8d.

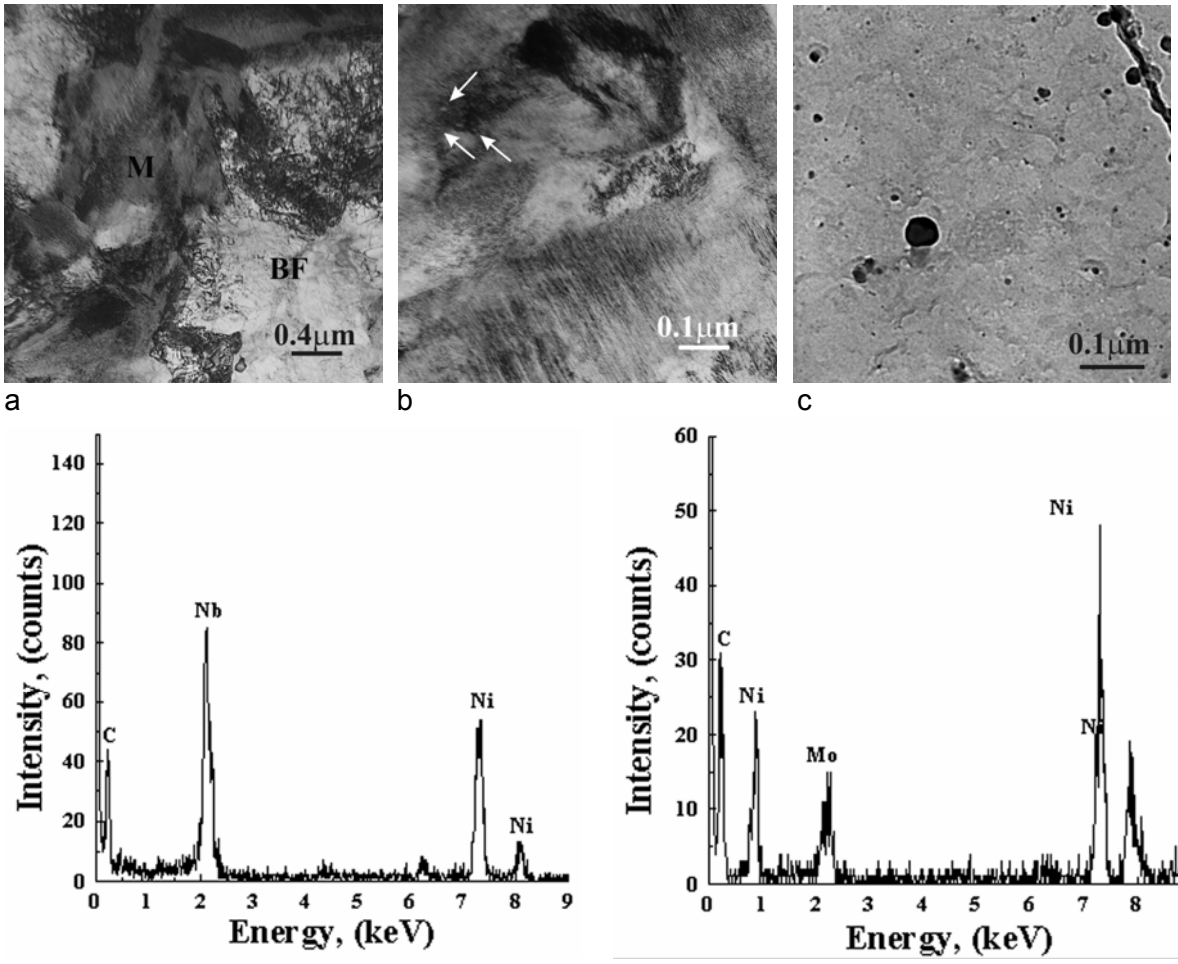

Fig. 6 Thin foil TEM micrographs (a,b) and carbon replica (c) showing the microstructure and precipitation in the NbMo steel after PS/BH. Representative energy dispersive X-ray spectrometer spectra (d,e) from the particles shown in c. M is martensite, BF is bainitic ferrite. Arrows in (b) indicate fine Fe_3C carbides. Note: Ni peaks are from Ni grid.

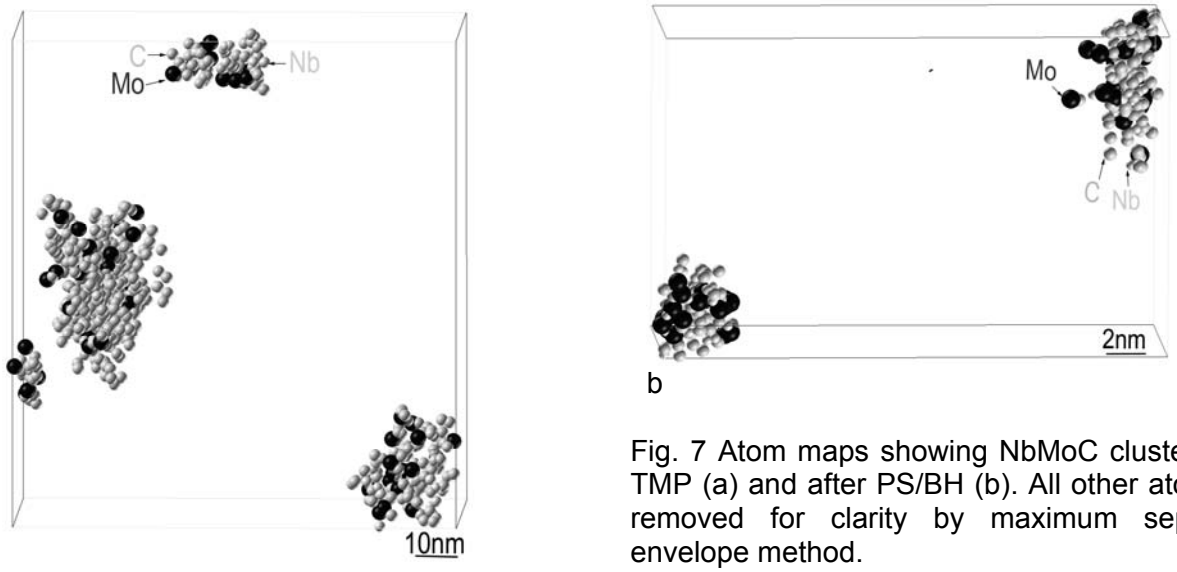

Fig. 7 Atom maps showing NbMoC clusters after TMP (a) and after PS/BH (b). All other atoms are removed for clarity by maximum separation envelope method.

Table 4. Average composition, Guinier radius and number densities of the clusters and precipitates in the PF/BF of NbMo steel as estimated using the maximum separation method from atom probe data.

	Composition, at% (AP)				AP		TEM		
	C	Mo	Nb	Fe	r_G, nm	N_v, m^{-3}	r, nm	d, nm	N_v, m^{-3}
TMP	25.0±0.8	4.4±0.4	6.8±0.5	60.0±0.9*	6.7±0.8	$1.7x10^{22}$	25±5	110±10	$6.2x10^{20}$
	53.6±3.0	6.9±1.5	11.5±2	26.6±2.6	4.1±0.7				
	45.6±9.3	29.5±8.8	14.3±6.5	10.2±4.9	1.9±0.3				
PF/BF	66.8±5.8	11.1±3.9	13.2±4.1	8.6±3.4	2.6±0.5				
	91.3±9.4	2.2±2.1	6.5±5.1	-	1.8±0.4				
TMP	71.0±2.3	1.1±0.5	1.3±0.6	24.8±2.2*	2.5	$6.3x10^{23}$			
	87.3±5.4	3.4±3.2	4.3±3.4	7.2±4.2	4.1±0.7				
Mar.	100	-	-	-	0.8±0.1				
PS/BH	43.4±1.7	7.9±0.9	18.4±1.4	27.7±1.6*	5.7	$1.7x10^{22}$	9±1.6	31±10	$8.3x10^{21}$
	54.2±3.8	13.7±2.6	20.0±3.0	11.8±2.5	3.2±0.1				
PF/BF	58.3±10.0	12.5±6.8	8.3±5.6	20.8±8.3	1.7				
PS/BH	100	-	-	-	0.9±0.2	$1.9x10^{24}$			
Mar.	93.2±4.1	-	-	6.4±3.9	1.1±0.3				
	81.3±4.8	-	-	17.7±4.7	1.4±0.6				
	61.4±1.9	0.1±0.1	0.05±0.05	36.6±1.9	2.7±0.2				
	49.1±1.2	0.2±0.1	0.08±0.06	47.3±1.2*	3.8±0.7				

* traces of Mn

Note: r_G is Guinier radius, r is the average radius of the particle determined by TEM, while d is average distance between the particles. N_v is number density.

Discussion

Both steels exhibited continuous yielding behaviour in TMP and TMP/PS/BH conditions. The yield strength increase after PS/BH treatment could be associated with several processes. One of them is an increase of dislocation density in (i) the PF and BF of both steels during pre-straining, (ii) localized strain hardening gradient in PF in the vicinity of hard RA and martensite islands, and (iii) in the surrounding martensite areas resulting from the volume change accommodation during strain-induced transformation of the RA to martensite. The formation of additional martensite islands, which are surrounded by the plastic deformation zones, in the PF leads to faster strain hardening of the PF and changes the partitioning of stress between the phases. The increased number density of dislocations leads to the higher work hardening of steels, as well as additional cluster and precipitation strengthening in the NbMo steel. The latter also resulted in an UTS increase. Formation of fine Fe_3C in the bainite of the non-Nb steel also contributed to precipitation strengthening of this steel. The dislocations that were formed during pre-straining could attract C atoms during BH, whereas the pre-existing Cottrell atmospheres after TMP could be further enriched in C. The latter could result in formation of clusters eventually leading to the precipitation of fine carbides on dislocations. Although the Cottrell atmospheres were observed in both the TMP and PS/BH conditions of non-Nb steel, no yield point appeared on the stress-strain curves. It is well known that the presence of the upper yield point on the strain-stress curves is the evidence of dislocations pinning in ferrite. In our case the steels contain a significant fraction of bainite, where the dislocation structure is more complex and of higher density compared to polygonal ferrite, so more carbon is needed to lock the dislocations in bainitic ferrite. In addition, due to the complex dislocation structure, there is no locking and unlocking mechanism during straining. Thus, an increase in yield strength is without appearance of upper yield point and it could be suggested that the contribution of dislocation locking to the mechanical properties of the non-Nb steel is minor compared to all other complex events taking place during plastic deformation of this multiphase steel, and which are responsible for its continuous yielding behaviour.

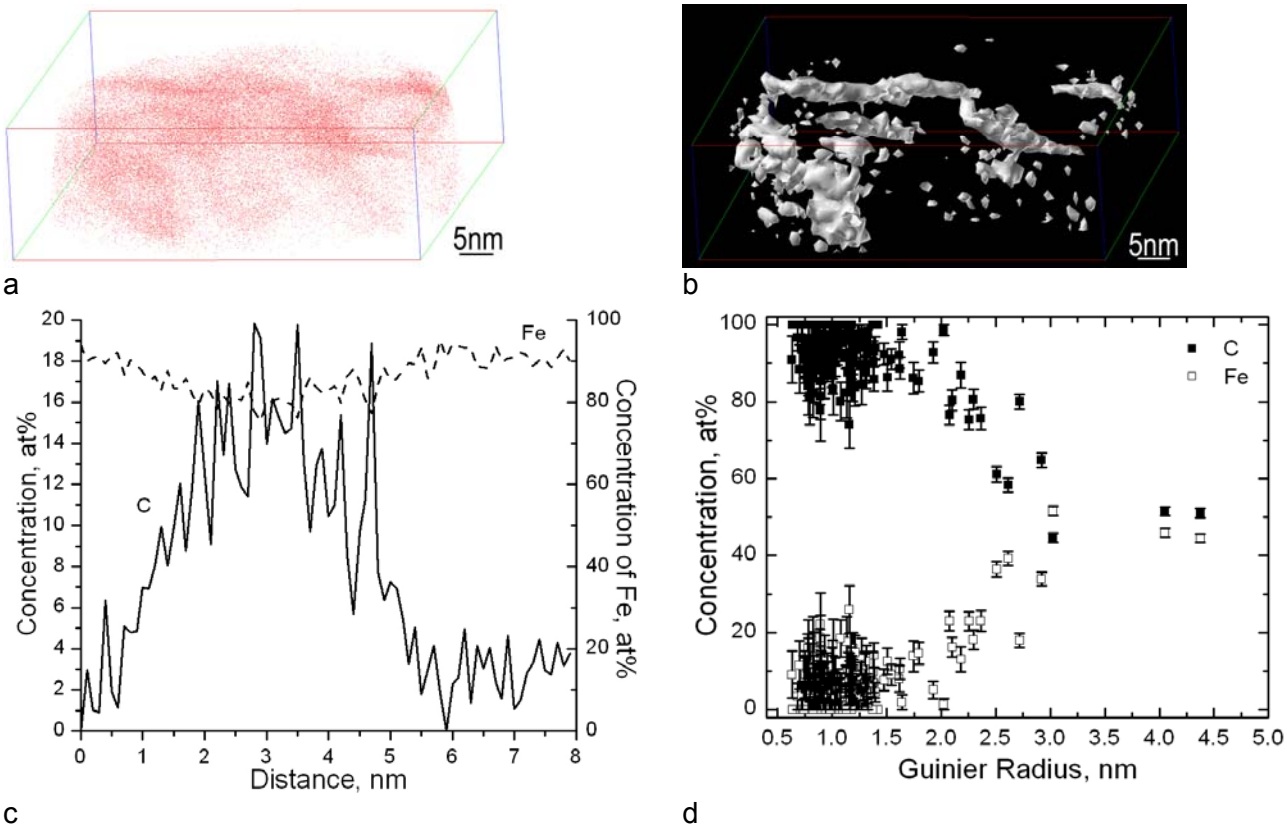

Fig. 8 C atom map (a), corresponding 9at%C iso-concentration surfaces (b) and representative concentration profiles across a carbide (c) showing formation of carbides in martensite of NbMo steel after PS/BH. Summary of variation of carbide composition with size is given in d.

The presence of Cottrell atmospheres at dislocations was observed only in the ferrite of the non-Nb steel. Although a significant number of alloyed TRIP steel samples was analysed in this and previous work [16,17], no dislocations that exhibited solute segregation were detected. This might be due to the higher binding energy of C atoms to Nb (2.3eV) compared to the binding energy of C atoms to dislocations (0.75eV) [18]. Therefore, there is a preference in formation of Nb-rich and Mo-rich C-Nb-Mo-Fe clusters and fine precipitates in the alloyed steels to the formation of C atmospheres at dislocations. The calculations of a number of carbon atoms per equivalent {112} and {222} planes in the atmospheres were performed by dividing the number of carbon atoms in the atmosphere by the number of these planes per dislocation length. The results are shown in Table 5. The choice of {112} and {222} iron-atom planes for examination was based on their resistance to dislocation glide, as their orientation is normal to the dislocation line of edge and screw dislocation, respectively [19]. The results are in agreement with the average C atoms concentration of 16±13 and 11±9 on {112} and {222} planes, respectively, obtained in our previous work [20]. These results are also in agreement with the theoretical predictions for saturation values of Cottrell atmospheres in ferrite [19].

The density of C clusters in the martensite was an order of magnitude higher than the density of C-Nb-Mo-Fe clusters/fine particles in the PF/BF of the NbMo steel. It was also slightly higher than the number density of C-rich clusters in the martensite of non-Nb steel (cf. Tables 3 and 4). The observed C-Mo-Nb-Fe clusters in the TMP condition changed their compositions during BH with the tendency towards an increased Nb and Mo content in the precipitates of similar C concentration. For example, in precipitates containing ~54 at. %C the concentration of Mo increased from ~7 to 14 at.%, while an average Nb content increased from ~12 to 20at%. This was accompanied by ~30-50% increase in

their dimensions (Table 4). The observed changes may be the result of pipe diffusion during the BH. No C-rich (>70 at. %) clusters were detected in the PS/BH samples, which could be associated with the tendency towards the stoichiometric (Nb,Mo)C composition. However, the APT data were rather limited and further work is required to support the above assumption.

Table 5 Characterisation of dislocations observed by APT in ferrite of the non-Nb steel after TMP

	Equivalent radius of dislocation, nm	**Maximum C content, at%**	**Number of C atoms per equivalent 112 plane**	**Number of C atoms per equivalent 222 plane**
Dislocation 1	4.7	9	28	20
Dislocation 2	1.84	4.5	17	12

Both steels exhibited decomposition of martensite with the formation of plate-like or rod-like iron carbides. The evolution of iron carbide composition with size was similar in both steels. Fine clusters contained 93-100 at. % C. With particle radius exceeding 1.2-1.4 nm, the C content decreased to 81-84 at. %. Further reduction to 62-64 at. % C is associated with a radius increase to 2.7-2.9 nm. The lowest C content detected in martensite of NbMo steel was ~49 at. % in the particles with an average radius of 3.8 nm. At the same time, the radius of the coarsest carbides observed in the non-Nb steel by APT was ~4.7 nm. These carbides contained ~24-25 at. % C, which correlates well with the composition of Fe_3C. It is likely that given more data collected for the NbMo steel, a similar trend toward the formation of Fe_3C particles with increasing size would be confirmed. It can be hypothesized that fine C-rich clusters serve as pre-cursors to the formation of iron carbides. It is interesting to note that some fine clusters in the PF/BF of the non-Nb steel after BH were observed with an average composition of Fe-~89 at. % C which corresponds to FeC_8. However, no carbides of this composition were observed in the martensite of both steels. As seen from the reported data, the composition of clusters and fine particles continuously changes with particle growth until a final composition of Fe_3C is reached. The number density of these clusters/fine carbides increased by an order of magnitude compared to the TMP condition. It was approximately the same for both steels. The decomposition of the martensite contributed to the high level of ductility maintained in these steels.

Conclusions

Significant YS and UTS increases were observed in both TRIP steels after PS/BH treatment. Although the ductility of both steels has decreased after PS/BH treatment, the total elongation values were still high. The observed changes in mechanical properties could be associated with (i) strain hardening of PF and BF as a result of pre-straining and strain-induced transformation of RA to martensite during pre-straining, (ii) precipitation hardening due to the formation of fine Fe_3C carbides in BF during BH and decomposition of martensite, and (iii) Nb-Mo-C cluster/precipitation strengthening in the NbMo steel.

Acknowledgement

The authors would like to thank Mrs. K.F. Russell from ORNL for technical assistance. This work was partially supported by Engineering Research Committee Grant, Monash University and University Research Committee Grant, University of Wollongong. Atom probe tomography research at the Oak Ridge National Laboratory SHaRE User Facility was sponsored by Basic Energy Sciences, U.S. Department of Energy (mkm, evp).

References

1. Y. Sakuma, O. Matsumura, H. Takechi. Metall. Mater. Trans. A, 1991, 22A: 489-498.
2. J Jacques, J. Ladrière, F. Delanny, Metall. Mater. Trans. A, 2001, 32A: 2759.
3. I.B. Timokhina, P.D. Hodgson, E.V. Pereloma, Metall. Mater. Trans. A, 2004, 35A: 2331-2341.
4. V.F. Zackay, E.R. Parker, D. Fahr, R. Bush, Trans. ASM, 1967, 60: 252-259.
5. B.C. De Cooman. Curr. Opin. Solid St. Mater. Sci. 2004;8:285.
6. K-I. Sugimoto, T. Muramatsu, S-I. Hashimoto, Y. Mukai, J. Mater. Process. Techn., 2006, 177: 390-395.
7. L.J. Baker, S.R. Daniel, J.D. Parker: Mater. Sci. Tech., 2002, 18: 355-68.
8. F.D. Bailey, R.P. Foley, D.K. Matlock DK. Symposium on High Strength Sheet Steels for the Automotive Industry. SAE, 1994, 119.
9. W. Bleck, S. Bruhl, T. Gerber, in *Steel - Future for the Automotive Industry*, Int. Conf. on Steels in Cars and Trucks - SCT 2005, 05.-10.06.2005, Wiesbaden. Ed. by I. von Hagen, H.-J. Wieland. Düsseldorf: Verlag Stahleisen 2005, S. 489-496.
10. I.B. Timokhina, E.V. Pereloma, P.D. Hodgson, Metall. Mater. Trans. A, 38A (2007), 2442-2454.
11. I.B. Timokhina, E.V. Pereloma, P.D. Hodgson, Mater. Sci. Forum, 2007, 539-547: 4315-4320.
12. I.B. Timokhina, M. Ryan, M.K. Miller, E.V. Pereloma, Iron and Steel, Suppl. 2005, 40:744-748.
13. M.K. Miller Atom Probe Tomography, in Handbook of Microscopy for Nanotechnology, eds. Nan Yao and Z.L. Wang, Kluwer Academic Press, New York, NY, 2005, p. 742.
14. P.B. Hirsch, A. Howie, R.B. Nicholson, D.W. Pashley and M.J. Whelan, Electron Microscopy of Thin Crystals, Butterworths, London, 1965, p. 422.
15. B.D. Cullity, Elements of X-Ray Diffraction, 2nd. ed., Addison-Wesley Publishing Company, Inc., 1978, pp.555.
16. E.V. Pereloma, I.B. Timokhina, M.K. Miller, P.D. Hodgson, Acta Mater. 2007, 55: 2587-2598.
17. E.V. Pereloma, I.B. Timokhina, K.F. Russell, M.K. Miller, Scripta Mater. 2006, 54:471-476.
18. A.W. Cochardt, G. Schoek, H. Wiedersich, Acta Metal., 1955; 3:533.
19. D. Kalish, M. Cohen. Mater.Sci. Eng. 1970 ; 6 :156.
20. E.V. Pereloma, I.B. Timokhina, J.J. Jonas, M.K. Miller, Acta Mater.2006, 54: 4539-4551.